

# 1            **Seismicity rate changes and geodetic transients in Central Apennines**

2

3 **Blaž Vičić<sup>1</sup>, Abdelkrim Aoudia<sup>1</sup>, Alessandra Borghi<sup>1,2</sup> Seyyedmaalek Momeni<sup>1</sup>, Alessandro**  
4 **Vuan<sup>3</sup>**

5

6 <sup>1</sup>The Abdus Salam International Centre for Theoretical Physics, Italy

7 <sup>2</sup>Istituto Nazionale Geofisica e Vulcanologia, sezione di Bologna, Italy

8 <sup>3</sup>National Institute of Oceanography and Applied Geophysics - OGS, Italy

9

10 Blaž Vičić ([bvicic@ictp.it](mailto:bvicic@ictp.it))

11

## 12 **Key Points:**

- 13        • Sub-horizontal shear zone beneath the shallow normal faults of Central Apennines is  
14        segmented into high and low seismicity rate strands
- 15        • Rate changes in seismicity are time-correlated with a transient deformation observed  
16        before the 2016 Central Italy sequence
- 17        • Mw5+ earthquakes on the Campotosto fault highlight a connection between high rate  
18        shear zone segments and locked fault patches

19

20

21 **Abstract**

22 Using template matching and GPS data, we investigate the evolution of seismicity and  
23 observable deformation in Central Apennines. Seismicity appears more persistent at the base of  
24 the seismogenic layer than in the shallower crust. Diffuse activity is reported on segments at  
25 depth, alternating along strike with apparent quiescence on segments that experienced one or  
26 more Mw6+ earthquakes in 1997, 2009 and 2016. Central Apennines are likely underlain by a  
27 sizeable shear zone with areas of diffuse seismicity bounding shallow normal faults where  
28 Mw6+ earthquakes occurred. The deformation observed at the surface seems to follow the  
29 seismicity variations at the base of seismogenic layer along the Apenninic chain. Principal and  
30 independent component analysis of GPS data exhibits a transient when the 2016 foreshock  
31 sequence starts. This transient propagated northward from the Campotosto fault up to the Alto  
32 Tiberina fault system and has likely loaded the Mw6+ 2016 earthquake sequence.

33

34 **Plain Language Summary**

35 We use a non-standard method for the detection of microseismicity at depth augmenting the  
36 available catalog. The enhanced seismicity distribution is coupled with the observable  
37 deformation on a geodetic network of continuous GPS to infer a better comprehension of the  
38 earthquake behaviour. The earthquake patterns in Central Apennines reveal a segmentation at  
39 depth along an almost flat base of seismogenic layer with alternating low and high seismicity  
40 rate segments. The deformation recorded at the surface seems to follow the seismicity variations  
41 at the base of seismogenic layer along the Apenninic chain also determining a possible seismic-  
42 aseismic mode. We suggest that aseismic deformation has a fundamental role in the tectonic  
43 loading and that seismicity, even if heterogeneously distributed, could represent a tracer of it.  
44 This conclusion is also supported by the evidence of a transient propagating from south to north  
45 during the 2016 Central Italy sequence.

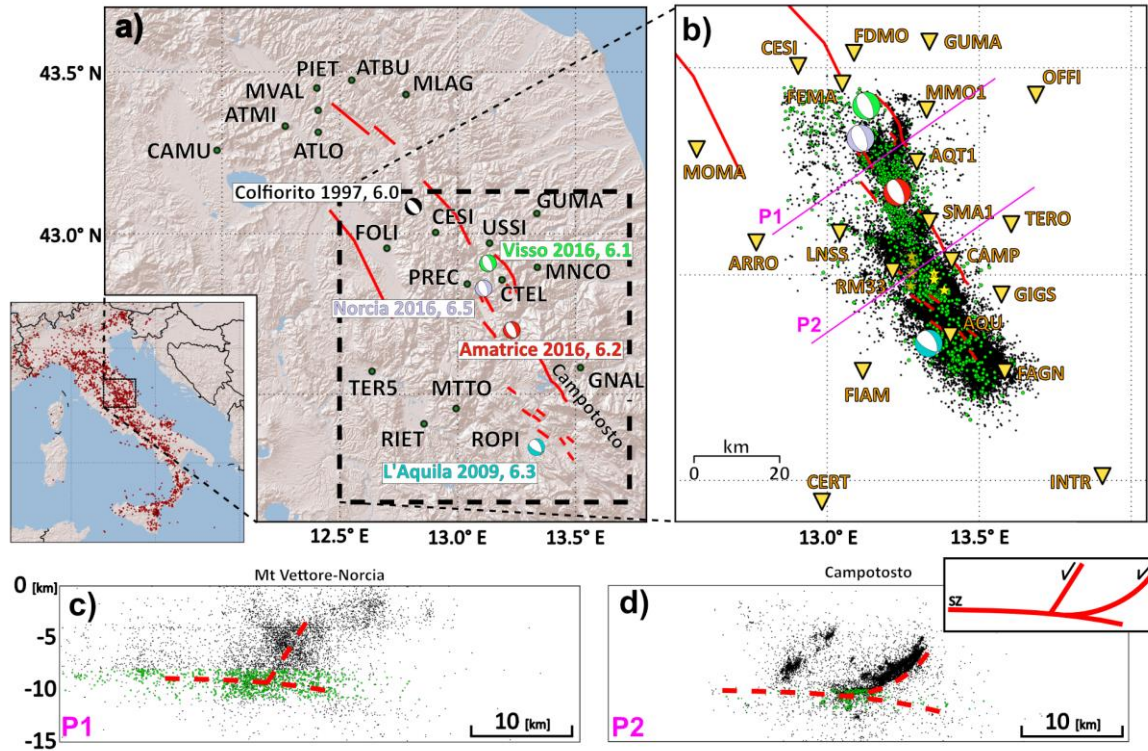
46

**47 1 Introduction**

48 Historical and recent destructive earthquakes in the Central Apennines, Italy (Amato et al., 1998;  
49 Chiaraluce et al., 2017; Rovida et al., 2011; Valoroso et al., 2013) occur mostly along the NW-  
50 SE trending system of normal faults, where 2 to 3 mm/year of extension perpendicular to the  
51 Apennines is accommodated (D'Agostino et al., 2011). The fault system is located above a  
52 delaminating Adria lithosphere (Aoudia et al. 2007; Chimera et al., 2003) within a complex  
53 tectonic setting (e.g. Calamita et al., 2003; Doglioni, 1991).

54 Central Apennines were recently struck by three destructive earthquake sequences, namely  
55 Umbria-Marche 1997, L'Aquila 2009 and Amatrice-Visso-Norcia 2016-2017. A large number of  
56 foreshocks and aftershocks was relocated using both continuous and temporary networks (Amato  
57 et al., 1998; Chiaraluce et al., 2003; Chiaraluce et al., 2011; Chiaraluce et al., 2017; Improta et  
58 al., 2019; Valoroso et al., 2013; Vuan et al., 2017) to depict the geometry of the system. The  
59 relocated catalogues of L'Aquila and Amatrice-Visso-Norcia sequences show a sub-horizontal  
60 and gently east-dipping Shear Zone (SZ) at the base of the seismogenic volume, between 8 and  
61 12 km. The sub-horizontal geometry of SZ is confirmed by focal solutions of foreshocks and  
62 aftershocks at the base of Campotosto and Monte Vettore faults (Chiaraluce et al., 2017; Improta  
63 et al., 2019; Valoroso et al., 2013). Deep seismic profiles and geologic cross-sections show a  
64 horizontal SZ between 8 and 11 km as a transition from sedimentary into basement units (e.g.  
65 Porreca et al. 2018). This transition corresponds to the observed velocity changes underneath  
66 L'Aquila and Amatrice-Visso-Norcia sequences as inferred by local earthquake travel-time  
67 tomography (Buttinelli et al. 2018; Chiarabba et al. 2018).

68 Before the L'Aquila 2009 mainshock, a foreshock sequence started in the area adjacent to the  
69 nucleation point of the Mw6.3 mainshock along the Paganica normal fault (Valoroso et al.,  
70 2013). Suga et al. (2014) identified three phases of foreshock migration towards the nucleation  
71 point of the April 6<sup>th</sup> 2009 mainshock, with one in mid-February interpreted as a slow-slip  
72 transient. The same transient was identified using GPS data by Borghi et al. (2016), who  
73 attributed it to a M6.1 slow-slip event. It was suggested that the transient took place over a sub-  
74 horizontal SZ at the base of Paganica and Campotosto faults involving the lateral extent of the  
75 aftershock sequence, causing stress loading close to the L'Aquila mainshock nucleation. Before  
76 the Amatrice, August 24<sup>th</sup> 2016 earthquake, Vuan et al. (2017) on the base of newly detected  
77 foreshocks, proposed that slip along the SZ increased the stress around the source area of the  
78 mainshock, therefore contributing to the unlocking of the overlying normal faults.



79  
80  
81  
82  
83  
84  
85  
Figure 1: Studied area of Central Italy. a) Map of destructive earthquakes since 1997 in the studied area. Beach ball colours refer to the same events in figure 1a, b. Red lines represent causative faults responsible for the mainshocks. In green we plot the continuous GPS stations. b) Triangles represent seismic stations used in this study. Black dots are earthquakes of 2009 L'Aquila and 2016 Amatrice-Visso-Norcia sequences. With green we show selected template earthquakes. c) and d) are cross-sections over Amatrice-Visso-Norcia and L'Aquila epicentral areas. In d) we show an idealized profile over the area with normal faults, mature listric faults and shear-zone.

86 Among the mentioned faults, the geometry and seismic potential of the Campotosto fault (Fig 1a,  
87 d) (hereafter Cf) for producing large earthquakes has been a matter of debate, especially after the  
88 occurrence of 2009 and 2016-2017 Mw5+ events (i.e. Chiaraluce et al., 2011; Cheloni et al.,  
89 2014; Cheloni et al., 2019; Falcucci et al., 2018; Gualandi et al., 2014; Valoroso et al., 2013).  
90 Cf is situated in the western flank of the Laga Mountains, oriented ~18km toward the northwest  
91 and dips toward the southwest with a listric geometry, as suggested from seismic data  
92 (Chiaraluce et al., 2011). This geometry was not retrieved from the GPS and InSAR studies  
93 (Cheloni et al., 2014; Cheloni et al., 2019; Falcucci et al., 2018; Gualandi et al., 2014) due to the  
94 quality of available data and methods used. Morpho-tectonic evidence confirms that Cf has  
95 different kinematics than its neighbouring Paganica and Mt Vettore-Norcia faults in its southeast  
96 and northwest, respectively, in term of fault slip rate (Falcucci et al., 2018). Cf is bounded at a  
97 depth of 10 km by SZ (Valoroso et al., 2013) and could be capable of producing an M6.4-6.6  
98 earthquake (Falcucci et al., 2018). Two historical earthquakes on Cf were reported (Galadini and  
99 Galli, 2003) over the past ~8 ka, with ~1 m of minimum vertical slip.  
100 Here we investigate both seismicity and deformation observed by the geodetic network of the  
101 Central Apennines. We exploit waveform similarity over 11 years from 2008 until the beginning  
102 of 2019 to define the spatial and temporal evolution of detected near-repeating earthquakes  
103 within the SZ and its relation to the reactivated normal faults. To better understand the geometry  
104 of Cf we invert the extended source ruptures of 8 ( $4.4 \leq M \leq 5.4$ ) earthquakes during the 2009 and  
105 2017 sequences (Fig 1b). We perform a principal component analysis and variational Bayesian

106 Independent Component Analysis of all available continuous GPS (cGPS) stations in the broader  
107 region of Central Apennines between January 1<sup>st</sup> 2015 until August 24<sup>th</sup> 2016 to detect possible  
108 geodetic transients and investigate their significance together with variations in seismicity. We  
109 study seismicity pattern of the SZ in the broader area of Central Apennines and compare it with  
110 our results for the 2009 and 2016 seismic sequences.

## 111 **2 Methods**

### 112 **2.1 Template matching**

113 We analyse the period from 2008 to the beginning of 2019 using only well relocated foreshocks  
114 and aftershocks of 2009 (Valoroso et al., 2013) and 2016 (Vuan et al., 2017) mainshocks (Fig  
115 1b). These selected events nucleated beneath the computed slip distribution of the mainshocks  
116 (Walters et al., 2018) within the SZ at depths between 10–12 km and 8–11 km for 2009 and 2016  
117 respectively. The merged earthquake catalog (Supplementary Material Fig S2, S3) was used in  
118 template matching (Gibbons & Ringdal, 2006; Ross et al., 2019; Shelly et al., 2007) to detect  
119 collocated near-repeating earthquakes and transients (Vičič et al., 2019) within the SZ. Daylong  
120 waveform data of selected stations (Fig 1b) are downsampled to 20 Hz and filtered between 2-8  
121 Hz. For each event, we compute the theoretical S-wave arrival time (Krischer et al., 2015) using  
122 a suitable velocity model (Herrmann et al., 2011) and trim the 3 component data in 5 seconds  
123 waveforms centred on this arrival. We extract the templates for the four closest stations. To  
124 detect new earthquakes we apply the template matching detection algorithm as described in  
125 Vuan et al. (2018). For positive detection we set a threshold of 12 times median absolute  
126 deviation of the daily stacked cross-correlation function. We only select detected events with  
127 inter-event times  $> 3$  seconds to not count same events as multiple events due to the detections  
128 from multiple templates. Selected detection inside this time window is the one with highest  
129 threshold value. The magnitude of the detection is calculated as the median value of the  
130 maximum amplitude ratio for all channels between the template and detected event where a 10-  
131 fold increase in amplitude corresponds to a unit increase in magnitude (Peng, et al. 2009).

### 132 **2.2 Extended source inversion**

133 We invert near-field three-component strong motion records of 8 earthquakes ( $4.4 \leq M \leq 5.4$ ) that  
134 occurred on the Cf during 2009 and 2017 sequences to study the kinematics of the ruptured area  
135 and constrain the geometry of Cf and discuss its seismogenic potential. The elliptical sub-fault  
136 approximation method (Di Carli et al., 2010; Twardzik et al., 2012; Ruiz & Madariaga, 2013;  
137 Momeni et al., 2019) is used to retrieve the robust features of the ruptures. For each rupture we  
138 look for the best waveform-fit to the observations (see Supplementary Material Figs. Sa1 to Sa7  
139 in Appendix-A) and infer the geometry of the Cf along strike and dip. The details of our  
140 inversions are presented in Appendix-A and B.

### 141 **2.3 GPS**

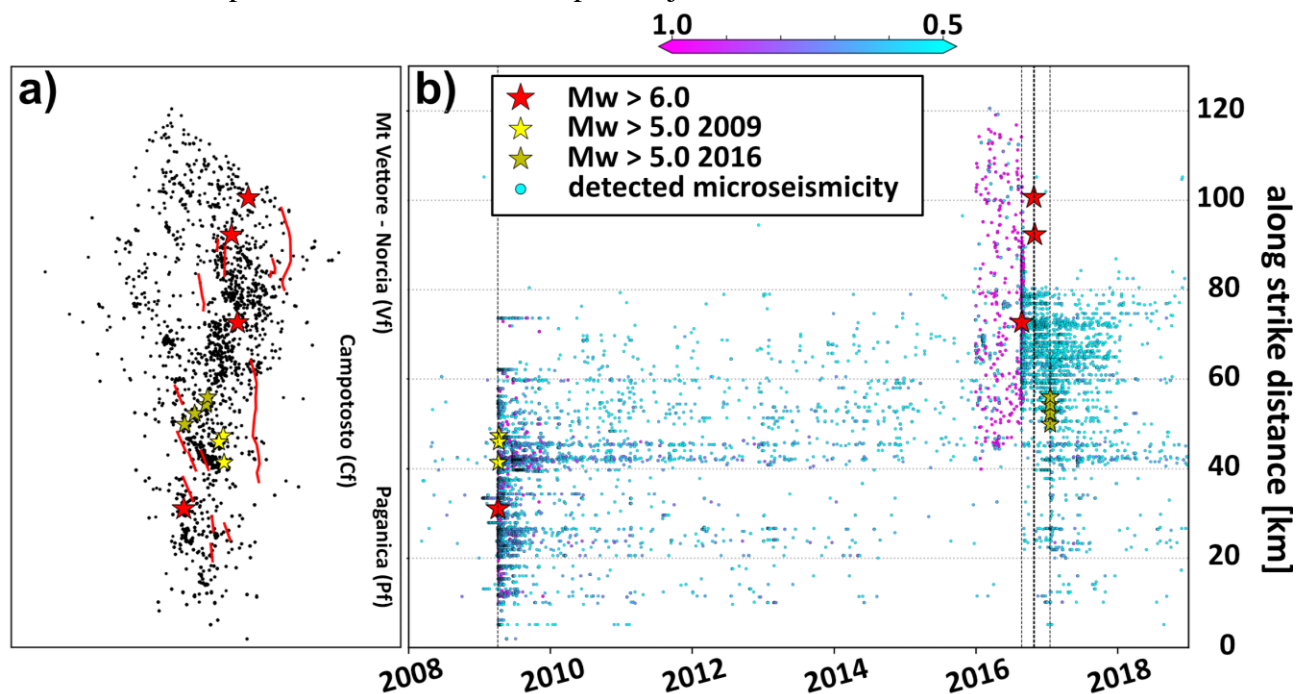
142 We perform a detailed analysis of the available cGPS stations along the Central Apennines from  
143 the Alto Tiberina fault system (ATF) to the north and area of L'Aquila 2009 earthquake to the  
144 south (Fig 1a). The 2015-2017 time series of the selected stations are analysed following the  
145 procedure described in Barzaghi and Borghi (2018) that includes the estimate of discontinuities  
146 due to station equipment changes, seismic events, periodic signals and a linear velocity term,  
147 considering the time correlation between data. The data were spatially filtered to remove

148 correlated noise using the Principal Component Analysis (PCA), as suggested by Dong et al.  
149 (2006) in order to search for transients (Borghetti et al., 2016; Gualandri et al., 2016). After the  
150 PCA, we apply variational Bayesian Independent Component Analysis (vbICA) (Choudrey et al.,  
151 2003) to solve for a blind source separation problem and study discontinuities in the time series.  
152 The methodology is described in the Supplementary Material (Appendix-C).  
153

154 **3 The 2009 – 2016 sequences**155 **3.1 Near-repeating earthquakes**

156 To evaluate spatial and temporal evolution of earthquake activity within the SZ, we used 1855  
 157 templates well distributed along strike and throughout the SZ beneath the causative faults of  
 158 2009 (10-12 km depth) and 2016-2017 (8-11 km depth) sequences (Fig 2a). We analyse the  
 159 continuous waveform series from 2008 to 2019, and detect 38229 near-repeaters in the SZ,  
 160 ranging between M-1.5 and M4.7 (Supplementary Fig S2).

161 Fig 2b shows the along-strike space-time distribution of the newly detected earthquakes (cross-  
 162 correlation values above 0.5). For the analysis, the whole SZ volume is divided into three sub-  
 163 volumes following the main normal faults: the Paganica fault (Pf), Cf and the Mt. Vettore-Norcchia  
 164 fault (Vf) (e.g. Basili et al., 2018). Beneath Pf, we detect the foreshocks to the L'Aquila  
 165 mainshock as reported in Sukan et al. (2014). After the L'Aquila mainshock, the detections  
 166 exhibit a decay of aftershocks as in Chiaraluce et al. (2011). On the contrary, diffuse and  
 167 continuous near-repeating earthquakes are reported within the SZ under the Cf (Fig 1a, d). We  
 168 separate the templates of 2016 sequence into foreshocks and early aftershocks (Supplementary  
 169 Fig S4a,b) inherent to the August 24<sup>th</sup> earthquake covering an 80 km along-strike distance that  
 170 includes Cf and Vf. For Cf, the detections reveal a continuous rate of activity, independent of the  
 171 templates we use, over the 11-year time span. Underneath Vf (Fig 1a, c), very few near-repeaters  
 172 are detected, except in its south-easternmost part, adjacent to Cf.



173  
 174 *Figure 2: a) Locations of selected SZ template earthquakes along strike the Central Italy faults activated in 2009 and 2016*  
 175 *sequences. b) Newly detected earthquakes from 2008 until the end of 2018. Colour represents the cross-correlation value of the*  
 176 *detection. 2009 sequence undergoes a decay of seismicity along the SZ of Paganica fault while the SZ underneath Campotosto*  
 177 *fault shows constant diffuse earthquake activity. At the beginning of 2016, foreshock activity of 2016 sequence start along the SZ*  
 178 *underneath Campotosto fault and SZ beneath Mt. Vettore fault system.*

179 The cumulative number of events over time and their yearly contributions are reported in Fig S5  
 180 and S6. We observe that soon after the 2009 mainshock and its aftershock sequence, earthquake  
 181 rate within the SZ beneath Cf overtakes (September 2009) the rate under the Pf. This is true

182 throughout the years 2010-2015, with few exceptions when a small sequence starts along Pf  
 183 (February 2011, February 2012, March 2013). The slope of earthquake rates beneath Cf is steady  
 184 over the years and characterizes the background seismicity with small increments over temporal  
 185 fluctuations (van den Ende et al., 2020).

186 At the end of 2015, the number of detections increased beneath Vf, starting the foreshock  
 187 sequence of the August 24<sup>th</sup> 2016 Mw6 earthquake. Beneath Cf an intensive swarm took place  
 188 during February 2016, located adjacent to the future termination of the mainshock slip  
 189 distribution (Chiaraluce et al., 2017). After the swarm, the SZ beneath Vf overtakes majority of  
 190 earthquake rate. The diffuse aftershocks that followed the August 24<sup>th</sup> mainshock are beneath Cf  
 191 and Vf, where most of the events took place. After the largest mainshock of October 30<sup>th</sup>, the  
 192 earthquake rate beneath Cf increases and by the end of 2016 seismic activity beneath Pf starts to  
 193 increase. Increased activity in late December 2016 beneath Cf signals the foreshock sequence of  
 194 the January 18<sup>th</sup> 2017 Mw5+ Campotosto earthquakes.

195 In Supplementary material (Fig S7) we plot earthquake activity in bins of 10 km along the strike  
 196 of the SZ beneath the fault system through time. We observe a slow (6 km/year) north-westward  
 197 migration of seismicity from the SZ beneath Pf towards the nucleation area of the August 24<sup>th</sup>  
 198 2016 mainshock. This is followed by a south-eastward migration (0.2 km/day) from the August  
 199 24<sup>th</sup> 2016 nucleation area towards the hypocentres of Campotosto 2017 earthquakes similar to  
 200 the observed migration of seismicity independent of the depth distribution reported by Sebastiani  
 201 et al. (2019).

### 202 **3.2 Rupture history for the CF moderate earthquakes**

203 The reported difference between coseismic and aseismic moment released along the Cf during  
 204 the 2009 and 2017 sequences (e.g. Cheloni et al., 2014; Cheloni et al., 2019) led to the detailed  
 205 investigation of the coseismic slip and source geometry of Mw5+ earthquakes on Cf.

206 Seven of the events (except the sub-horizontal June 22<sup>nd</sup> 2009  $M_L$ 4.4 event along SZ) occurred  
 207 on planes with strikes ranging from 142° to 190°, on average 157°, dipping to the southwest  
 208 (Supplementary Appendix-A Table A1). Our results confirm the listric geometry of Cf with dip  
 209 changing over depth from 50° to 30° (Supplementary Fig S1).

210 All slip models cover an area of ~18 km per 12 km on the Cf. The patches of maximum slip do  
 211 not overlap, and the ruptures evolved mostly up-dip. Similar to the migration observed along the  
 212 SZ after 2009 and 2016 sequence, also the 2009 and 2017 Campotosto Mw5+ events follow a  
 213 similar pattern and migrate from southeast towards northwest after 2009 and vice-versa after  
 214 2016. Unilateral ruptures are confirmed by directivity in the accelerograms.

215 Source parameters of the 2009 sequence show an average strike of 152° and dip of 48° for the  
 216 south-eastern part of the Cf. Scalar seismic moment of  $1.73 \cdot 10^{17}$  Nm for the three large  
 217 aftershocks and the SZ event of 2009 are close to the value of  $1.8 \cdot 10^{17}$  Nm, obtained using  
 218 point source inversion method by Scognamiglio et al. (2010). Using SAR and GPS data, Cheloni  
 219 et al., (2014) obtained a cumulative scalar seismic moment of  $3.17 \cdot 10^{17}$  Nm for co and post-  
 220 seismic phases in 2009 and Gualandi et al., 2014 calculated an afterslip of a  $2.9 \cdot 10^{17}$  Nm  
 221 released for 301 days after the 2009 mainshock. This suggests that most of the deformation was  
 222 aseismic with half as post-seismic considering negligible sum of the seismic moments released  
 223 by the rest of aftershocks (Falcucci et al., 2018).

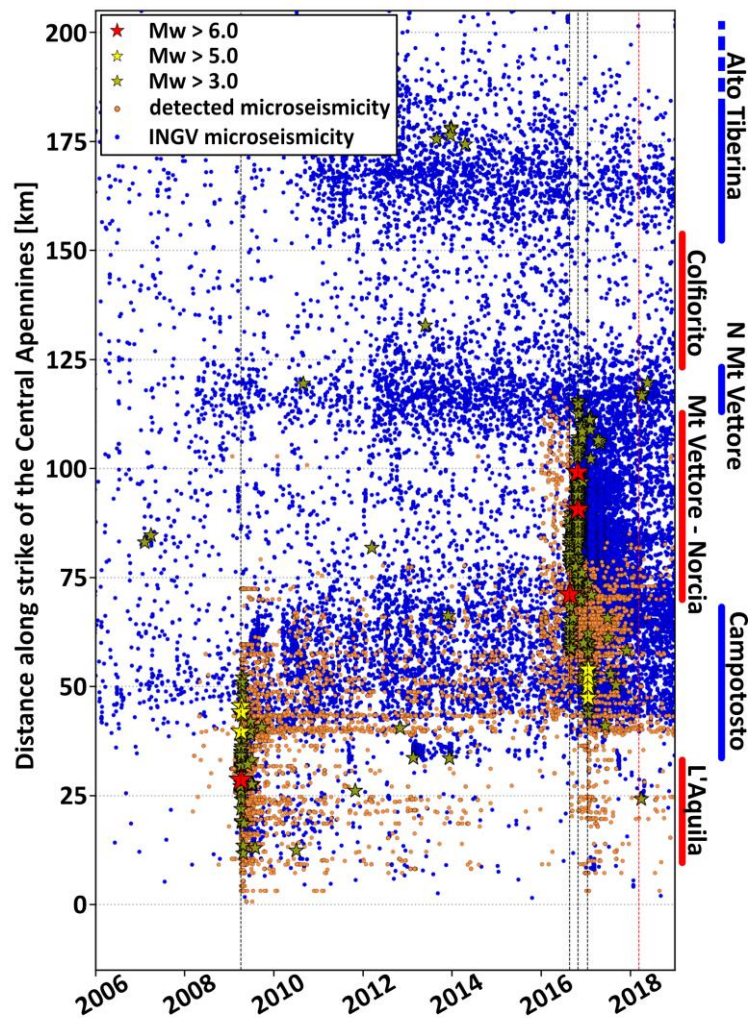
224 Average strike for the 2017 events ( north-western part of the Cf) is 161° while average dip is  
 225 35°, 13° less than Falcucci et al., (2018) from inversion of surface deformation measured from  
 226 cGPS and DInSAR. In their study, the rake angle would play an important role in obtaining the

227 dip angle, while in our inversions the rake was a well-retrieved parameter. The slip models  
228 distribute from depths of 2.5 km to 10 km with a maximum slip of 0.49 m close to Falcucci et al.,  
229 (2018). We obtain  $7.98 \cdot 10^{17}$  Nm of scalar seismic energy release during 2017 sequence close  
230 to the obtained value by Falcucci et al. (2018). Considering  $0.4 \cdot 10^{17}$  Nm of scalar seismic  
231 moment released by  $3.5 < M < 4.9$  aftershocks and the cumulative geodetic moment of  $9.29 \cdot 10^{17}$   
232 Nm (Cheloni et al., 2019), we reach to the same 35% contribution of aseismic strain release  
233 suggested by Cheloni et al., (2019).

234 The computed slip history of the Mw5+ events indicate that Cf is partially reactivated along its  
235 deeper extent and a rupture up to the surface would require a larger magnitude earthquake as  
236 reported by paleoseismologic observations (e.g. Galadini et al., 2003).  
237

238 **4 Central Apennines**239 **4.1 Seismicity**

240 We compare our newly constrained catalog with the Italian Seismic Bulletin (Fig 3). We remove  
 241 earthquakes shallower than 12 km (removing fixed depth and shallow events) along the Central  
 242 Apennines. We observe alternating high and low seismicity rate strands along the strike, showing  
 243 similarities to our own findings in the SZ beneath Pf, Cf and Vf. The areas of last moderate  
 244 earthquakes in 1997, 2009 and 2016 correspond to strands where seismicity is less diffuse. The  
 245 high seismicity rate segments are located in between, namely Campotosto segment, North Mt.  
 246 Vettore segment (NVf), and Alto Tiberina segment (Anderlini et al., 2016).  
 247

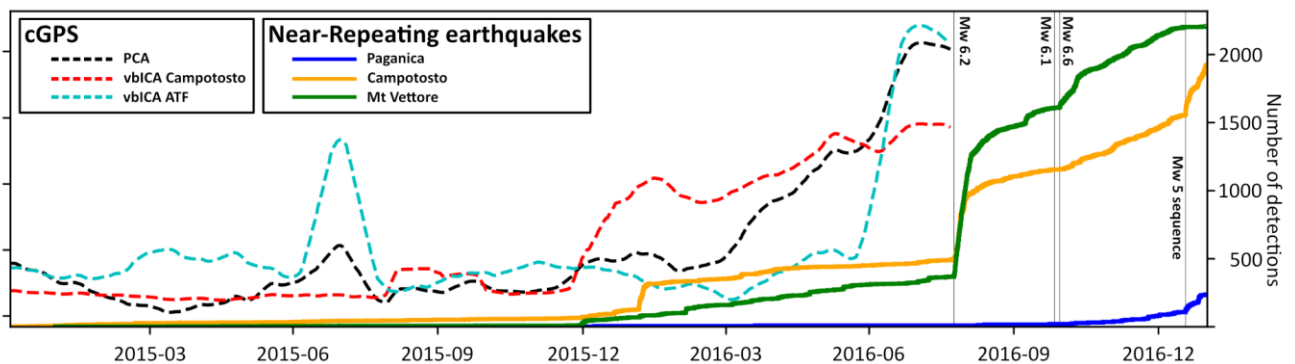


248  
 249 *Figure 3: Seismicity along the strike of Central Apennines. Orange dots represents the near-repeating earthquakes obtained in*  
 250 *this study while blue dots represent earthquakes deeper than 12 km from INGV earthquake catalog. We observe good spatial*  
 251 *correlation between our enhanced catalog in the 2009 and 2016 epicentral areas and INGV catalog. Additionally, similar*  
 252 *behaviour is observed along strike of the Central Apennines. Along the segmented SZ we observe segments of high rate seismicity*  
 253 *(Campotosto, N. Mt. Vettore, Alto Tiberina – blue vertical lines on the right) and segments with low rate of seismicity (L'Aquila,*  
 254 *Mt. Vettore-Norcia, Colfiorito – red vertical lines on the right). Later correspond to the SZ beneath the faults, that ruptured with*  
 255 *recent Mw 6+ events.*

## 256 4.2. GPS analysis

257 The analysed GPS network is reported in Fig. 1a. The central part of the network, where the  
 258 2016 M6+ events nucleated represents an empty zone since no stations were installed in that  
 259 period or we do not have access to the data. Although the vbICA method has resulted efficient in  
 260 finding the signal along the Alto Tiberina fault (ATF) (Gualandi et al., 2017), we also applied the  
 261 PCA method, as it allows finding the average behaviour of the stations and avoids local effects.  
 262 We show the results (Fig. 4) in terms of the second Principal Component (PC2) of the East  
 263 component. We observe an increase of values starting at the beginning of 2016 with both  
 264 northern (ATF) and southern (Campotosto) GPS station cluster contributing to the PC2. We  
 265 repeat the analysis splitting the stations in the ATF and in the Campotosto part. Analysing the  
 266 two clusters separately allowed us to point out a similar behaviour of the ATF and Campotosto  
 267 stations but shifted in time: the Campotosto stations present this discontinuity in the first vbICA  
 268 component on January 7<sup>th</sup> 2016, with a probability around 94% as detected by the Bayesian test  
 269 inference (Appendix-C), whereas the ATF stations present an analogous behaviour seven months  
 270 later on July 7<sup>th</sup> with a probability of 98% (Fig 4). The last analysis involves the cGPS stations  
 271 set up after the Mw6.5 October 30<sup>th</sup> 2016 earthquake. The time-series show (Appendix-C Fig  
 272 Sc2) the non-linear effect of the post-seismic deformation. Accordingly we preferred not to fit  
 273 the data using any functional models but applied the PCA to describe the deformation. In  
 274 Appendix-C Fig Sc2 the first and second principal components are reported. All the stations are  
 275 affected by a common signal represented by the linear tectonic rate and the post-seismic  
 276 deformations, as shown by the first PC (Appendix-C Fig Sc2), however a discontinuity is present  
 277 at the beginning of 2018. Soon after the discontinuity, the northern extension of the area affected  
 278 by 3 Mw6+ earthquakes is hit by a series of Mw3.5+ earthquakes with the strongest Mw4.5 on  
 279 April 10<sup>th</sup> 2018.

280



281 *Figure 4: Cumulative number of newly detected near repeating earthquakes between 2015 and 2017 and a geodetic transient.*  
 282 *Different colours represent different segments of SZ under the shallow normal faults. Dashed black line represents 2nd principal*  
 283 *component over all the GPS stations used while red and magenta represent independent components of spatially grouped cGPS*  
 284 *stations, around Campotosto and ATF respectively. We observe that deformation is migrating from the south of the system*  
 285 *towards north.*  
 286

287

288 **5 Conclusions**

289  
290 Analysing 11 years of continuous waveforms recorded at multiple seismic stations in Central  
291 Italy allowed us to detect more than 38.000 near-repeaters within the shear zone (SZ). The  
292 detected events and their locations give us insight on the space-time behaviour of the SZ  
293 underneath Paganica fault (Pf), Campotosto fault (Cf) and Monte Vettore fault (Vf) before, after  
294 and in-between the recent Central Italy earthquake sequences. Pf and Vf are related to the 2009  
295 Mw6.1 L'Aquila earthquake and the 2016 Amatrice-Visso-Norcia Mw6+ earthquakes  
296 respectively, which ruptured shallow, SW dipping normal faults. Cf, located in between Pf and  
297 Vf, is affected in the aftermath of both 2009 and 2016 sequences with earthquakes of Mw5+.  
298 We observe different spatial and temporal patterns of earthquakes within the SZ underneath Pf,  
299 Cf and Vf.

300 The seismicity rate within the SZ appears to be segmented from south to north along the strike of  
301 the fault system (Fig 3). SZ beneath Pf is experiencing an expected decay in its activity after the  
302 2009 earthquake reaching a lower rate with very few events after 2014 while the adjacent SZ  
303 beneath Cf exhibits a far higher rate in its activity that is continuous over time. The SZ beneath  
304 Vf shows a very low rate between 2009 up to the end of 2015 when it starts exhibiting a large  
305 foreshock sequence, also affecting SZ beneath Cf and Vf as well as the above normal faults,  
306 prior to the 2016 Mw6+ earthquakes.

307 Our study suggests that Central Apennines are underlain by a sizeable sub-horizontal shear zone  
308 that is segmented in its frictional and/or mechanical properties accommodating therefore low and  
309 high rates of seismicity at the base of the seismogenic layer. The low rate seismicity segments  
310 are beneath high-angle normal faults responsible of the 1997, 2009 and 2016 earthquake  
311 sequences. The high rate seismicity segments are beneath listric faults (e.g. Campotosto), and  
312 low-angle normal faults (e.g. Alto-Tiberina).

313 Analysing 19 cGPS stations show that the start of the 2016 foreshock sequence coincides with a  
314 clear geodetic transient that first affected Cf-Pf and later expanded northward affecting ATF. The  
315 foreshock near-repeaters likely correspond to creeping patches accommodating aseismic slow-  
316 slip in the foreshock period (e.g. Meng et al., 2014) combined with a gradual unlocking within  
317 the plate boundary (e.g. Schurr et al., 2014). The space-time correlations between the seismicity  
318 and the geodetic transient and their northward along strike migrations are thus most likely due to  
319 an expanding/propagating slow-slip along strike. Our results show that the northward expanding  
320 transient was accommodated differently by the segmented system where less-coupled and  
321 creeping segments connect areas of future large earthquakes. Similar behaviour is described in  
322 subduction zones (e.g. Rolandone et al., 2018; Radiguet et al., 2016). Furthermore, we argue that  
323 the geometry and the frictional properties of the segmented system affects the degree of  
324 interseismic coupling. This likely leads to differences in recurrence intervals and maximum  
325 magnitude between mature listric faults and younger high-angle normal faults as exhibited by the  
326 historical seismicity and paleoseismology across Central Apennines (e.g. Cinti et al., 2018;  
327 Falcucci et al., 2018; Galadini et al., 2003; Galli et al., 2019; Guidoboni et al., 2018).

328

329 **Acknowledgments**

330

331 The authors would like to thank Generali group and Generali Italia for the financial support.

332 PyMPA software (Vuan et al., 2018) development is partly supported by the project “Real-time

333 earthquake risk reduction for a resilient Europe” (RISE), financed by the Horizon 2020

334 programme of the European Commission.

335 The data are available via the European Integrated Data Archive managed by Istituto Nazionale

336 di Geofisica e Vulcanologia (INGV) (<http://www.orfeus-eu.org/webdc3/>).

337

338 **References**

- 339  
340 Amato, A., Azzara, R., Chiarabba, C., Cimini, G. B., Cocco, M., Di Bona, M., ... & Basili, A.  
341 (1998). The 1997 Umbria-Marche, Italy, earthquake sequence: A first look at the main shocks  
342 and aftershocks. *Geophysical Research Letters*, 25(15), 2861-2864,  
343 <https://doi.org/10.1029/98GL51842>  
344
- 345 Anderlini, L., Serpelloni, E., & Belardinelli, M. E. (2016). Creep and locking of a low-angle  
346 normal fault: Insights from the Altotiberina fault in the Northern Apennines (Italy). *Geophysical*  
347 *Research Letters*, 43(9), 4321-4329, <https://doi.org/10.1002/2016GL068604>  
348
- 349 Aoudia, A., Ismail-Zadeh, A. T., & Romanelli, F. (2007). Buoyancy-driven deformation and  
350 contemporary tectonic stress in the lithosphere beneath Central Italy. *Terra Nova*, 19(6), 490-  
351 495, <https://doi.org/10.1111/j.1365-3121.2007.00776.x>  
352
- 353 Barzaghi, R., & Borghi, A. (2018). Theory of second order stationary random processes applied  
354 to GPS coordinate time-series. *GPS Solutions*, 22(3), 86, [https://doi.org/10.1007/s10291-018-](https://doi.org/10.1007/s10291-018-0748-4)  
355 [0748-4](https://doi.org/10.1007/s10291-018-0748-4)  
356
- 357 Basili, R., Burrato, P., Fracassi, U., Kastelic, V., Maesano, F., Tarabusi, G., ... & DISS Working  
358 Group. (2018). Database of Individual Seismogenic Sources (DISS), Version 3.2. 1: A  
359 compilation of potential sources for earthquakes larger than M 5.5 in Italy and surrounding areas,  
360 <https://doi.org/10.6092/INGV.IT-DISS3.2.1>  
361
- 362 Borghi, A., Aoudia, A., Javed, F., & Barzaghi, R. (2016). Precursory slow-slip loaded the 2009  
363 L'Aquila earthquake sequence. *Geophysical Journal International*, 205(2), 776-784,  
364 <https://doi.org/10.1093/gji/ggw046>  
365
- 366 Buttinelli, M., Pezzo, G., Valoroso, L., De Gori, P., & Chiarabba, C. (2018). Tectonics  
367 inversions, fault segmentation, and triggering mechanisms in the central Apennines normal fault  
368 system: Insights from high-resolution velocity models. *Tectonics*, 37(11), 4135-4149,  
369 <https://doi.org/10.1029/2018TC005053>  
370
- 371 Calamita, F., Paltrinieri, W., Pelorosso, M., Scisciani, V., & Tavarnelli, E. (2003). Inherited  
372 mesozoic architecture of the Adria continental palaeomargin in the Neogene central Apennines  
373 orogenic system, Italy. *BOLLETTINO-SOCIETA GEOLOGICA ITALIANA*, 122(2), 307-318.  
374
- 375 Cheloni, D., Giuliani, R., D'Anastasio, E., Atzori, S., Walters, R. J., Bonci, L., ... & Deninno, F.  
376 (2014). Coseismic and post-seismic slip of the 2009 L'Aquila (central Italy) Mw 6.3 earthquake  
377 and implications for seismic potential along the Campotosto fault from joint inversion of high-  
378 precision levelling, InSAR and GPS data. *Tectonophysics*, 622, 168-185,  
379 <https://doi.org/10.1016/j.tecto.2014.03.009>  
380  
381  
382

- 383 Cheloni, D., D'Agostino, N., Scognamiglio, L., Tinti, E., Bignami, C., Avallone, A., ... &  
 384 Mattone, M. (2019). Heterogeneous Behavior of the Campotosto Normal Fault (Central Italy)  
 385 Imaged by InSAR GPS and Strong-Motion Data: Insights from the 18 January 2017  
 386 Events. *Remote Sensing*, 11(12), 1482, <https://doi.org/10.3390/rs11121482>  
 387
- 388 Chiarabba, C., De Gori, P., Cattaneo, M., Spallarossa, D., & Segou, M. (2018). Faults geometry  
 389 and the role of fluids in the 2016–2017 Central Italy seismic sequence. *Geophysical Research*  
 390 *Letters*, 45, 6963–6971. <https://doi.org/10.1029/2018GL077485>  
 391
- 392 Chiaraluce, L., Ellsworth, W. L., Chiarabba, C., & Cocco, M. (2003). Imaging the complexity of  
 393 an active normal fault system: The 1997 Colfiorito (central Italy) case study. *Journal of*  
 394 *Geophysical Research: Solid Earth*, 108(B6), <https://doi.org/10.1029/2002JB002166>  
 395
- 396 Chiaraluce, L., Valoroso, L., Piccinini, D., Di Stefano, R., & De Gori, P. (2011). The anatomy of  
 397 the 2009 L'Aquila normal fault system (central Italy) imaged by high resolution foreshock and  
 398 aftershock locations. *Journal of Geophysical Research: Solid Earth*, 116(B12),  
 399 <https://doi.org/10.1029/2011JB008352>  
 400
- 401 Chiaraluce, L., Di Stefano, R., Tinti, E., Scognamiglio, L., Michele, M., Casarotti, E., ... &  
 402 Lombardi, A. (2017). The 2016 central Italy seismic sequence: A first look at the mainshocks,  
 403 aftershocks, and source models. *Seismological Research Letters*, 88(3), 757-771,  
 404 <https://doi.org/10.1785/0220160221>  
 405
- 406 Chimera, G., Aoudia, A., Saraò, A., & Panza, G. F. (2003). Active tectonics in Central Italy:  
 407 constraints from surface wave tomography and source moment tensor inversion. *Physics of the*  
 408 *Earth and Planetary Interiors*, 138(3-4), 241-262, [https://doi.org/10.1016/S0031-](https://doi.org/10.1016/S0031-9201(03)00152-3)  
 409 [9201\(03\)00152-3](https://doi.org/10.1016/S0031-9201(03)00152-3)  
 410
- 411 Choudrey, R. A., & Roberts, S. J. (2003). Variational mixture of Bayesian independent  
 412 component analyzers. *Neural computation*, 15(1), 213-252,  
 413 <https://doi.org/10.1162/089976603321043766>  
 414
- 415 Cinti, F. R., Civico, R., Blumetti, A. M., Chiarini, E., La Posta, E., Pantosti, D., ... & Pinzi, S.  
 416 (2018). Evidence for surface faulting earthquakes on the Montereale fault system (Abruzzi  
 417 Apennines, central Italy). *Tectonics*, 37(9), 2758-2776, <https://doi.org/10.1029/2017TC004780>  
 418
- 419 D'Agostino, N., Mantenuto, S., D'Anastasio, E., Giuliani, R., Mattone, M., Calcaterra, S., ... &  
 420 Bonci, L. (2011). Evidence for localized active extension in the central Apennines (Italy) from  
 421 global positioning system observations. *Geology*, 39(4), 291-294,  
 422 <https://doi.org/10.1130/G31796.1>  
 423
- 424 Di Carli, S., François-Holden, C., Peyrat, S., & Madariaga, R. (2010). Dynamic inversion of the  
 425 2000 Tottori earthquake based on elliptical subfault approximations. *Journal of Geophysical*  
 426 *Research: Solid Earth*, 115(B12), <https://doi.org/10.1029/2009JB006358>  
 427

- 428 Doglioni, C. (1991). A proposal for the kinematic modelling of W-dipping subductions-possible  
 429 applications to the Tyrrhenian-Apennines system. *Terra Nova*, 3(4), 423-434,  
 430 <https://doi.org/10.1111/j.1365-3121.1991.tb00172.x>  
 431
- 432 Dong, D., Fang, P., Bock, Y., Webb, F., Prawirodirdjo, L., Kedar, S., & Jamason, P. (2006).  
 433 Spatiotemporal filtering using principal component analysis and Karhunen-Loeve expansion  
 434 approaches for regional GPS network analysis. *Journal of geophysical research: solid*  
 435 *earth*, 111(B3), <https://doi.org/10.1029/2005JB003806>.  
 436
- 437 Falcucci, E., Gori, S., Bignami, C., Pietrantonio, G., Melini, D., Moro, M., ... & Galadini, F.  
 438 (2018). The Campotosto seismic gap in between the 2009 and 2016–2017 seismic sequences of  
 439 central Italy and the role of inherited lithospheric faults in regional seismotectonic  
 440 settings. *Tectonics*, 37(8), 2425-2445, <https://doi.org/10.1029/2017TC004844>  
 441
- 442 Galadini, F., & Galli, P. (2003). Paleoseismology of silent faults in the Central Apennines (Italy):  
 443 the Mt. Vettore and Laga Mts. faults. *Annals of Geophysics*, <https://doi.org/10.4401/ag-3457>  
 444
- 445 Galli, P., Galderisi, A., Peronace, E., Giaccio, B., Hajdas, I., Messina, P., ... & Polpetta, F.  
 446 (2019). The awakening of the dormant Mount Vettore fault (2016 central Italy earthquake, Mw  
 447 6.6): paleoseismic clues on its millennial silences. *Tectonics*, 38(2), 687-705,  
 448 <https://doi.org/10.1029/2018TC005326>  
 449
- 450 Gibbons, S. J., & Ringdal, F. (2006). The detection of low magnitude seismic events using array-  
 451 based waveform correlation. *Geophysical Journal International*, 165(1), 149-166,  
 452 <https://doi.org/10.1111/j.1365-246X.2006.02865.x>  
 453
- 454 Gualandi, A., Serpelloni, E., & Belardinelli, M. E. (2014). Space–time evolution of crustal  
 455 deformation related to the M w 6.3, 2009 L'Aquila earthquake (central Italy) from principal  
 456 component analysis inversion of GPS position time-series. *Geophysical Journal*  
 457 *International*, 197(1), 174-191, <https://doi.org/10.1093/gji/ggt522>  
 458
- 459 Gualandi, A., Serpelloni, E., & Belardinelli, M. E. (2016). Blind source separation problem in  
 460 GPS time series. *Journal of Geodesy*, 90(4), 323-341, [https://doi.org/10.1007/s00190-015-0875-](https://doi.org/10.1007/s00190-015-0875-4)  
 461 [4](https://doi.org/10.1007/s00190-015-0875-4)  
 462 Gualandi, A., Nichele, C., Serpelloni, E., Chiaraluce, L., Anderlini, L., Latorre, D., ... & Avouac,  
 463 J. P. (2017). Aseismic deformation associated with an earthquake swarm in the northern  
 464 Apennines (Italy). *Geophysical Research Letters*, 44(15), 7706-7714,  
 465 <https://doi.org/10.1002/2017GL073687>  
 466
- 467 Guidoboni, E., Ferrari, G., Mariotti, D., Comastri, A., Tarabusi, G., Sgattoni, G., & Valensise, G.  
 468 (2018). CFTI5Med, Catalogo dei Forti Terremoti in Italia (461 aC-1997) e nell'area  
 469 Mediterranea (760 aC-1500), <https://doi.org/10.6092/ingv.it-cfti5>  
 470
- 471 Herrmann, R. B., Malagnini, L., & Munafò, I. (2011). Regional Moment Tensors of the 2009  
 472 L'Aquila Earthquake Sequence Regional Moment Tensors of the 2009 L'Aquila Earthquake

- 473 Sequence. *Bulletin of the Seismological Society of America*, 101(3), 975-993,  
 474 <https://doi.org/10.1785/0120100184>
- 475 Improta, L., Latorre, D., Margheriti, L., Nardi, A., Marchetti, A., Lombardi, A. M., ... & Moretti,  
 476 M. (2019). Multi-segment rupture of the 2016 Amatrice-Visso-Norcia seismic sequence (central  
 477 Italy) constrained by the first high-quality catalog of Early Aftershocks. *Scientific reports*, 9(1),  
 478 1-13, <https://doi.org/10.1038/s41598-019-43393-2>
- 479
- 480 Krischer, L., Megies, T., Barsch, R., Beyreuther, M., Lecocq, T., Caudron, C., & Wassermann, J.  
 481 (2015). ObsPy: A bridge for seismology into the scientific Python ecosystem. *Computational*  
 482 *Science & Discovery*, 8(1), 014003, <https://doi.org/10.1088/1749-4699/8/1/014003>
- 483
- 484 Meng, L., Huang, H., Bürgmann, R., Ampuero, J. P., & Strader, A. (2015). Dual megathrust slip  
 485 behaviors of the 2014 Iquique earthquake sequence. *Earth and Planetary Science Letters*, 411,  
 486 177-187, <https://doi.org/10.1016/j.epsl.2014.11.041>
- 487
- 488 Momeni, S. M., Aoudia, A., Tatar, M., Twardzik, C., & Madariaga, R. (2019). Kinematics of the  
 489 2012 Ahar–Varzaghan complex earthquake doublet (M w6. 5 and M w6. 3). *Geophysical*  
 490 *Journal International*, 217(3), 2097-2124, <https://doi.org/10.1093/gji/ggz100>
- 491
- 492 Peng, Z., & Zhao, P. (2009). Migration of early aftershocks following the 2004 Parkfield  
 493 earthquake. *Nature Geoscience*, 2(12), 877-881, <https://doi.org/10.1038/ngeo697>
- 494
- 495 Porreca, M., Minelli, G., Ercoli, M., Brobia, A., Mancinelli, P., Cruciani, F., ... & Cannata, A.  
 496 (2018). Seismic reflection profiles and subsurface geology of the area interested by the 2016–  
 497 2017 earthquake sequence (Central Italy). *Tectonics*, 37(4), 1116-1137,  
 498 <https://doi.org/10.1002/2017TC004915>
- 499
- 500 Radiguet, M., Perfettini, H., Cotte, N., Gualandi, A., Valette, B., Kostoglodov, V., ... &  
 501 Campillo, M. (2016). Triggering of the 2014 M w 7.3 Papanao earthquake by a slow slip event in  
 502 Guerrero, Mexico. *Nature Geoscience*, 9(11), 829-833, <https://doi.org/10.1038/ngeo2817>
- 503
- 504 Rolandone, F., Nocquet, J. M., Mothes, P. A., Jarrin, P., Vallée, M., Cubas, N., ... & Font, Y.  
 505 (2018). Areas prone to slow slip events impede earthquake rupture propagation and promote  
 506 afterslip. *Science advances*, 4(1), eaao6596, <https://doi.org/10.1126/sciadv.aao6596>
- 507
- 508 Ross, Z. E., Trugman, D. T., Hauksson, E., & Shearer, P. M. (2019). Searching for hidden  
 509 earthquakes in Southern California. *Science*, 364(6442), 767-771,  
 510 <https://doi.org/10.1126/science.aaw6888>
- 511
- 512 Rovida, A., Camassi, R., Gasperini, P., & Stucchi, M. (2011). Catalogo parametrico dei terremoti  
 513 italiani, <https://doi.org/10.13127/CPTI/CPTI15.2>
- 514
- 515 Ruiz, S., & Madariaga, R. (2013). Kinematic and dynamic inversion of the 2008 Northern Iwate  
 516 earthquake. *Bulletin of the Seismological Society of America*, 103(2A), 694-708,  
 517 <https://doi.org/10.1785/0120120056>
- 518

- 519 Schmedes, J., Archuleta, R. J., & Lavallée, D. (2010). Correlation of earthquake source  
520 parameters inferred from dynamic rupture simulations. *Journal of Geophysical Research: Solid*  
521 *Earth*, 115(B3), <https://doi.org/10.1029/2009JB006689>  
522
- 523 Schurr, B., Asch, G., Hainzl, S., Bedford, J., Hoechner, A., Palo, M., ... & Oncken, O. (2014).  
524 Gradual unlocking of plate boundary controlled initiation of the 2014 Iquique earthquake.  
525 *Nature*, 512(7514), 299-302, <https://doi.org/10.1038/nature13681>  
526
- 527 Scognamiglio, L., Tinti, E., Michelini, A., Dreger, D. S., Cirella, A., Cocco, M., ... & Piatanesi,  
528 A. (2010). Fast determination of moment tensors and rupture history: What has been learned  
529 from the 6 April 2009 L'Aquila earthquake sequence. *Seismological Research Letters*, 81(6),  
530 892-906, <https://doi.org/10.1785/gssrl.81.6.892>  
531
- 532 Sebastiani, G., Govoni, A., & Pizzino, L. (2019). Aftershock Patterns in Recent Central  
533 Apennines Sequences. *Journal of Geophysical Research: Solid Earth*, 124(4), 3881-3897,  
534 <https://doi.org/10.1029/2018JB017144>  
535
- 536 Shelly, D. R., Beroza, G. C., & Ide, S. (2007). Non-volcanic tremor and low-frequency  
537 earthquake swarms. *Nature*, 446(7133), 305-307, <https://doi.org/10.1038/nature05666>  
538
- 539 Soldati, G., Zaccarelli, L., Faenza, L., & Michelini, A. (2015). Monitoring of crustal seismic  
540 velocity variations in the L'Aquila fault zone inferred from noise cross-correlation. *Geophysical*  
541 *Journal International*, 202(1), 604-611, <https://doi.org/10.1093/gji/ggv172>  
542
- 543 Sugan, M., Kato, A., Miyake, H., Nakagawa, S., & Vuan, A. (2014). The preparatory phase of  
544 the 2009 Mw 6.3 L'Aquila earthquake by improving the detection capability of low-magnitude  
545 foreshocks. *Geophysical Research Letters*, 41(17), 6137-6144,  
546 <https://doi.org/10.1002/2014GL061199>  
547
- 548 Twardzik, C., Madariaga, R., Das, S., & Custódio, S. (2012). Robust features of the source  
549 process for the 2004 Parkfield, California, earthquake from strong-motion  
550 seismograms. *Geophysical Journal International*, 191(3), 1245-1254,  
551 <https://doi.org/10.1111/j.1365-246X.2012.05653.x>  
552
- 553 Valoroso, L., Chiaraluce, L., Piccinini, D., Di Stefano, R., Schaff, D., & Waldhauser, F. (2013).  
554 Radiography of a normal fault system by 64,000 high-precision earthquake locations: The 2009  
555 L'Aquila (central Italy) case study. *Journal of Geophysical Research: Solid Earth*, 118(3), 1156-  
556 1176, <https://doi.org/10.1002/jgrb.50130>  
557
- 558 van den Ende, M. P., & Ampuero, J. P. (2020). On the statistical significance of foreshock  
559 sequences in Southern California. *Geophysical Research Letters*, 47(3), e2019GL086224.  
560
- 561 Vičić, B., Aoudia, A., Javed, F., Foroutan, M., & Costa, G. (2019). Geometry and mechanics of  
562 the active fault system in western Slovenia. *Geophysical Journal International*, 217(3), 1755-  
563 1766, <https://doi.org/10.1093/gji/ggz118>  
564

- 565 Vuan, A., Sukan, M., Chiaraluce, L., & Di Stefano, R. (2017). Loading rate variations along a  
566 midcrustal shear zone preceding the Mw6. 0 earthquake of 24 August 2016 in Central Italy.  
567 *Geophysical Research Letters*, 44(24), <https://doi.org/10.1002/2017GL076223>  
568
- 569 Vuan, A., Sukan, M., Amati, G., & Kato, A. (2018). Improving the Detection of Low-Magnitude  
570 Seismicity Preceding the M w 6.3 L’Aquila Earthquake: Development of a Scalable Code Based  
571 on the Cross Correlation of Template Earthquakes. *Bulletin of the Seismological Society of*  
572 *America*, 108(1), 471-480, <https://doi.org/10.1785/0120170106>  
573
- 574 Walters, R. J., Gregory, L. C., Wedmore, L. N. J., Craig, T. J., McCaffrey, K., Wilkinson, M., ...  
575 & Iezzi, F. (2018). Dual control of fault intersections on stop-start rupture in the 2016 Central  
576 Italy seismic sequence. *Earth and Planetary Science Letters*, 500, 1-14,  
577 <https://doi.org/10.1016/j.epsl.2018.07.043>  
578

579 **References From the Supporting Information**

580

581 Blewitt, G., Hammond, W. C., & Kreemer, C. (2018). Harnessing the GPS data explosion for  
582 interdisciplinary science. *Eos*, 99, 1-2, <https://doi.org/10.1029/2018EO104623>.

583

584 Borghi A., Aoudia A., Riva R., Barzaghi R. (2009). GPS monitoring and earthquake prediction:  
585 a success story towards a useful integration. *Tectonophysics*, 465, pp 177-189, ISSN 0040-1951,  
586 doi: 10.1016/j.tecto.2008.11.022

587

588 Borghi, A., Cannizzaro, L., & Vitti, A. (2012). Advanced techniques for discontinuity detection  
589 in GNSS coordinate time-series. An Italian case study. In *Geodesy for Planet Earth*(pp. 627-  
590 634). Springer, Berlin, Heidelberg , [https://doi.org/10.1007/978-3-642-20338-1\\_77](https://doi.org/10.1007/978-3-642-20338-1_77)

591

592 Cotton, F., & Coutant, O. (1997). Dynamic stress variations due to shear faults in a plane-layered  
593 medium. *Geophysical Journal International*, 128(3), 676-688, [https://doi.org/10.1111/j.1365-  
594 246X.1997.tb05328.x](https://doi.org/10.1111/j.1365-246X.1997.tb05328.x)

595

596 Hyvärinen, A., & Oja, E. (2000). Independent component analysis: algorithms and  
597 applications. *Neural networks*, 13(4-5), 411-430, [https://doi.org/10.1016/S0893-6080\(00\)00026-  
598 5](https://doi.org/10.1016/S0893-6080(00)00026-5)

599

600 Sambridge, M. (1999). Geophysical inversion with a neighbourhood algorithm—I. Searching a  
601 parameter space. *Geophysical journal international*, 138(2), 479-494,  
602 <https://doi.org/10.1046/j.1365-246X.1999.00876.x>

603

604 Sambridge, M. (1999). Geophysical inversion with a neighbourhood algorithm—II. Appraising  
605 the ensemble. *Geophysical Journal International*, 138(3), 727-746,  
606 <https://doi.org/10.1046/j.1365-246x.1999.00900.x>

607

608 Silverii, Francesca, et al. "Transient crustal deformation from karst aquifers hydrology in the  
609 Apennines (Italy)." *Earth and Planetary Science Letters* 506 (2019): 23-37,  
610 <https://doi.org/10.1016/j.epsl.2018.10.019>

611

612 Spudich, P., & Miller, D. P. (1990). Seismic site effects and the spatial interpolation of  
613 earthquake seismograms: results using aftershocks of the 1986 North Palm Springs, California,  
614 earthquake. *Bulletin of the Seismological Society of America*, 80(6A), 1504-1532.

615

Figure 1.

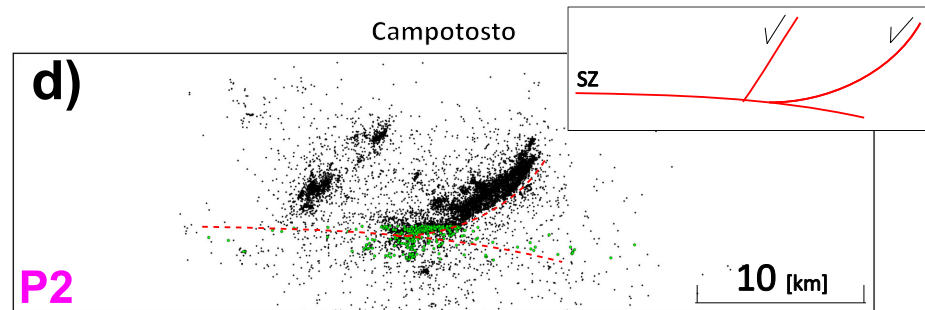
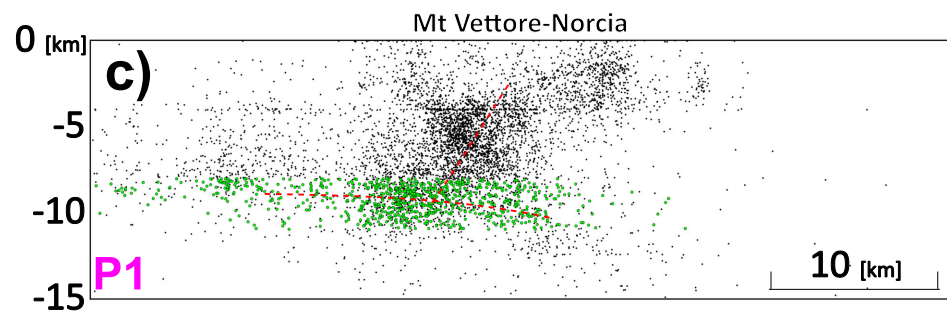
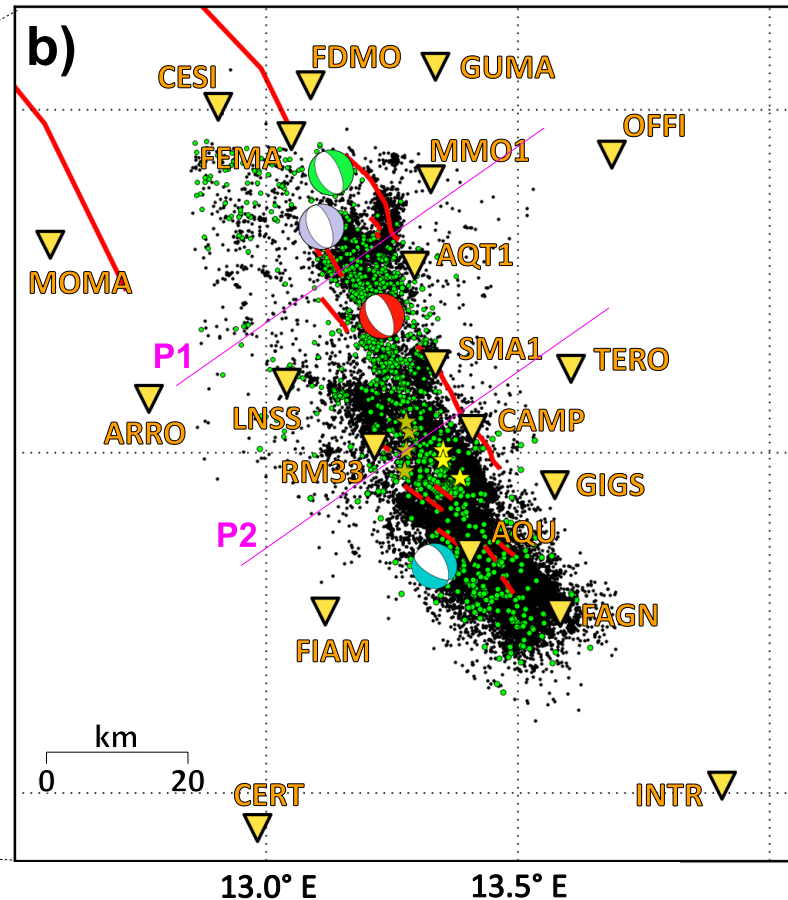
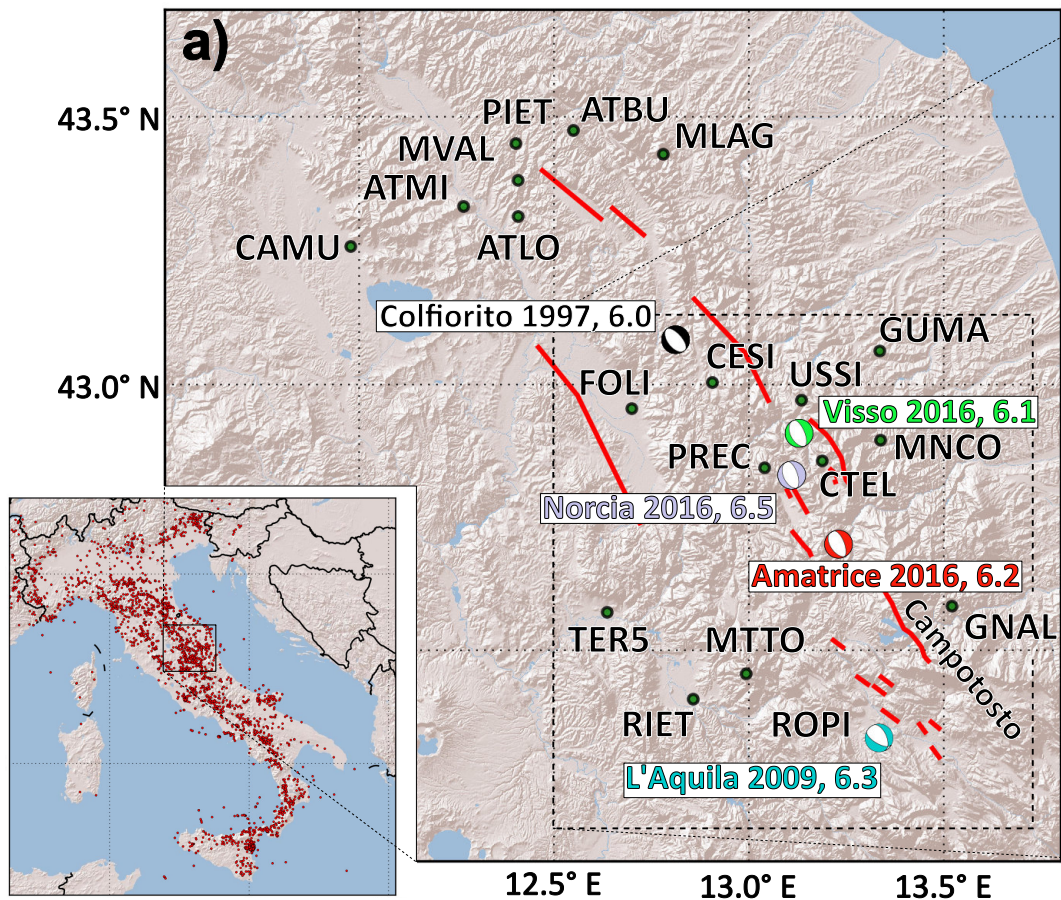


Figure 2.

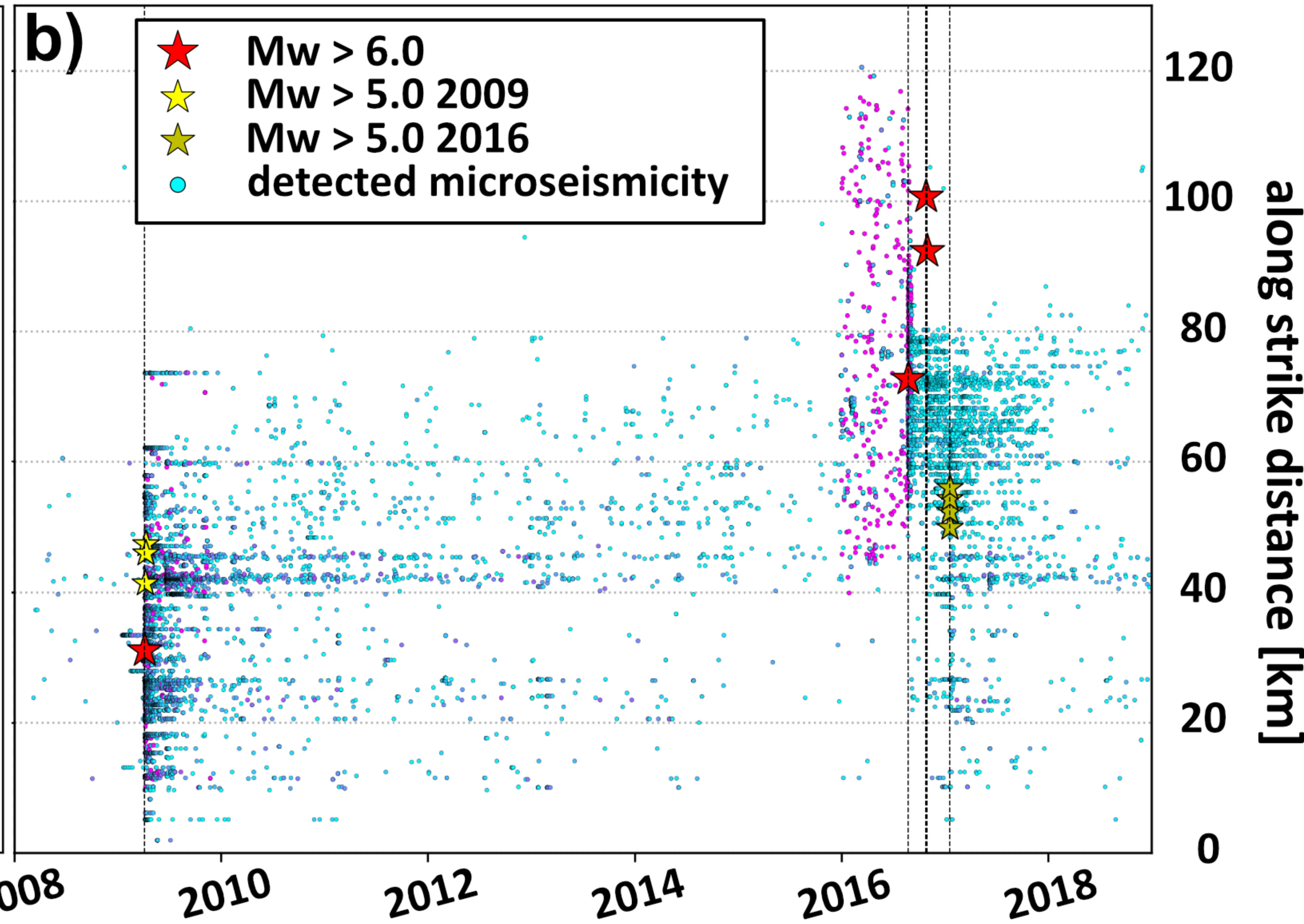
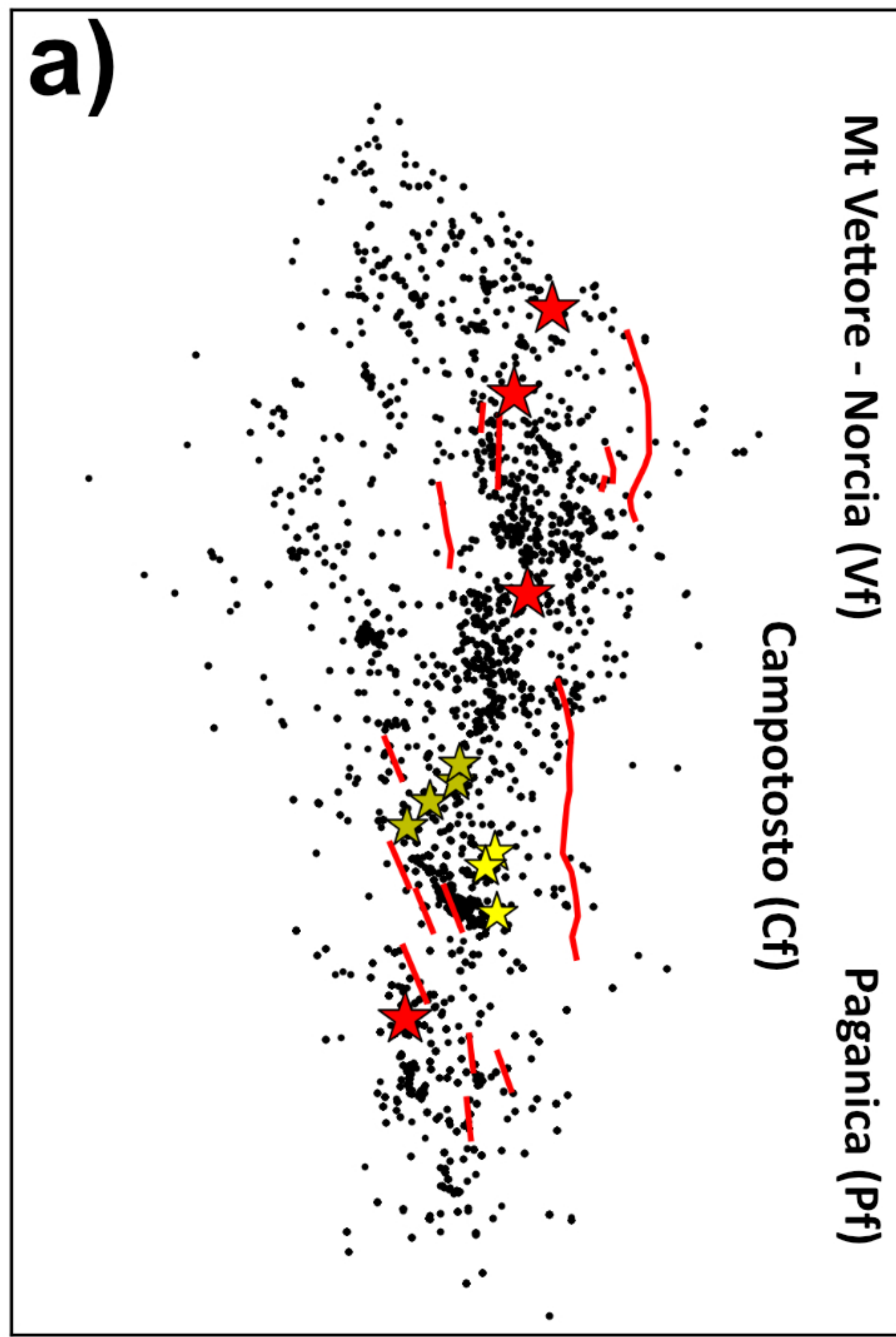
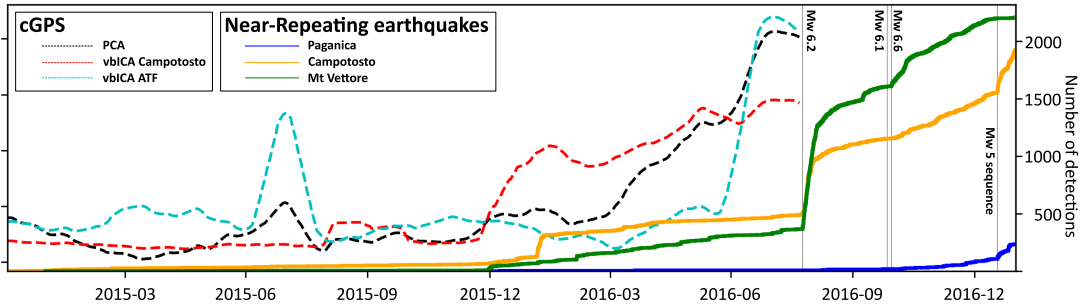


Figure 3.



**Figure 4.**

